Journal of
Plankton Research

academic.oup.com/plankt

J. Plankton Res. (2019) 41(4): 521–533. First published online July 30, 2019 doi:10.1093/plankt/fbz033

ORIGINAL ARTICLE

A comparison between *Zooglider* and shipboard net and acoustic mesozooplankton sensing systems

BENJAMIN M. WHITMORE, CATHERINE F. NICKELS AND MARK D. OHMAN
SCRIPPS INSTITUTION OF OCEANOGRAPHY, UNIVERSITY OF CALIFORNIA SAN DIEGO, LA JOLLA, CA 92093, USA

*CORRESPONDING AUTHOR: bmwhitmo@ucsd.edu

Received January 12, 2019; editorial decision May 13, 2019; accepted June 11, 2019

Corresponding editor: John Dolan

Some planktonic patches have markedly higher concentrations of organisms compared to ambient conditions and are <5 m in thickness (i.e. thin layers). Conventional net sampling techniques are unable to resolve this vertical microstructure, while optical imaging systems can measure it for limited durations. *Zooglider*, an autonomous zooplankton-sensing glider, uses a low-power optical imaging system (Zoocam) to resolve mesozooplankton at a vertical scale of 5 cm while making concurrent physical and acoustic measurements (Zonar). In March 2017, *Zooglider* was compared with traditional nets (MOCNESS) and ship-based acoustics (Simrad EK80). Zoocam recorded significantly higher vertically integrated abundances of smaller copepods and appendicularians, and larger gelatinous predators and mineralized protists, but similar abundances of chaetognaths, euphausiids, and nauplii. Differences in concentrations and size-frequency distributions are attributable to net extrusion and preservation artifacts, suggesting advantages of *in situ* imaging of organisms by *Zooglider*. Zoocam detected much higher local concentrations of copepods and appendicularians (53 000 and 29 000 animals m^{-3}, respectively) than were resolvable by nets. The EK80 and Zonar at 200 kHz agreed in relative magnitude and distribution of acoustic backscatter. The profiling capability of *Zooglider* allows for deeper high-frequency acoustic sampling than conventional ship-based acoustics.

KEYWORDS: Zooglider; mesozooplankton; vertical microstructure; patchiness; thin layers

available online at academic.oup.com/plankt

INTRODUCTION

When observed at fine (1–10 m) and micro (<1 m) scales, the vertical structure of planktonic ecosystems is highly patchy (Haury *et al.*, 1978), and thin layers are common. Thin layers have been defined as recurrent and persistent fine-scale features (<5 m in vertical extent) that have elevated concentrations (e.g. three times the ambient concentration) of organisms, chlorophyll or particles (Dekshenieks *et al.*, 2001). These layers and patches can have significant ecological consequences within the planktonic community, such as predatory behavioral changes (Benoit-Bird, 2009), increased encounter rates between predators and prey or between potential mates, differential grazing rates (Menden-Deuer and Grünbaum 2006), enhanced water column productivity (Rovinsky *et al.*, 1997; Brentnall *et al.*, 2003) and altered carbon cycling (Pinel-Alloul and Ghadouani, 2007; Wilson and Steinberg 2010; Prairie *et al.*, 2015).

Zooplankton vertical structure is currently investigated with three basic approaches: acoustic backscatter, physical collection, and optical imaging. Each sampling method has unique benefits and limitations. Acoustic backscatter methods can approximate biomass, are less susceptible to organismal avoidance and can sample great volumes of water quickly. However, the acoustic sensing of zooplankton is complicated by several factors (e.g. target taxonomic composition, target orientation, material properties of organisms, and frequency-dependence of acoustic backscatter), and targets cannot be identified explicitly (McGehee *et al.*, 1998; Griffiths *et al.*, 2002), unless the acoustic system is complemented with a net or imaging system (Briseño-Avena *et al.*, 2015).

Net tows and plankton pumps physically retain organisms, allow for species-level classification, and with proper preservation the physical specimens can be examined, DNA sequenced, or analyzed for stable isotopes or other properties long after their initial collection date. All types of physical sample collection have associated financial constraints (e.g. ship-time, sample preservation and archiving, and processing time), which severely limit the number of samples that can be obtained and processed. Advances in image processing, including the ZooImage (Grosjean and Denis, 2007), the ZooScan (Gorsky *et al.*, 2010) and the Flowcam (Fluid Imaging Technologies), have helped to improve the post-processing time of net, pump and bottle-collected samples. However, physical collection systems are still hindered by systematic limitations. Pump systems such as CALPS (Pitois *et al.*, 2016) and CUFES (Checkley *et al.*, 1997) are mounted to the hull of a ship and can sample continuously while the ship is underway, but only at a single depth. Like traditional open nets, opening–closing nets give a sample integrated over a horizontal distance and depth range when towed obliquely (MOCNESS; Wiebe *et al.*, 1985) or strictly a depth range when towed vertically (Multi-net; Weikert and John, 1981). Opening–closing nets are superior to traditional nets as they can isolate the vertical component of the plankton community in smaller bins (vertical resolution is generally $\geq\sim$10 m); however, that resolution is not sufficient to resolve the multiple scales of patchiness and predator–prey interactions in the planktonic environment (Möller *et al.*, 2012). Nets can also damage delicate organisms (Hamner *et al.*, 1975; Omori and Hamner 1982), while other organisms dissolve in the preservation solution if not properly treated (Beers and Stewart 1970). Some planktonic organisms, such as euphausiids, exhibit net avoidance behavior (Brinton, 1967; Wiebe *et al.*, 1982), while other zooplankton are extruded through net mesh (Nichols and Thompson 1991; Remsen *et al.*, 2004; Skjoldal *et al.*, 2013) and are thus underrepresented in samples.

Optical imaging systems can discern the identity or shape profile of organisms; however, the volume sampled is much smaller than acoustic, net and pump-based systems. Imaging systems differ widely in image resolution, capture rate, sample volume, and deployment method. Particle counters (e.g. laser optical particle counter) are only able to discern the rough shape profile of objects within the water column (Herman *et al.*, 2004). The 3D imaging systems utilize either multiple cameras or a single holographic camera to reveal the 3D orientation and identity of an organism in sample volumes ranging from much less than 1 mL to 2 L (Sheng *et al.*, 2003; Wiebe and Benfield, 2003). Several additional imaging systems are also in use for plankton recognition that sample larger volumes of water at slightly lower resolution, e.g. *IS*IIS (Cowen and Guigand, 2008), LOKI (Schulz *et al.*, 2009), SCP (Roberts *et al.*, 2014), UVP (Picheral *et al.*, 2010), Video Plankton Recorder (VPR) (Davis *et al.*, 2005) and ZOOVIS (Trevorrow *et al.*, 2005).

The specific configuration of these instruments on profiling devices or towed bodies can markedly affect the avoidance responses of the targeted zooplankton. Any instrument moving through the water will generate a hydrodynamic disturbance to some degree. For planktonic organisms, this disturbance can induce escape responses if it exceeds an organism-specific shear threshold (Haury *et al.* 1980; Fields and Yen 1997; Buskey *et al.*, 2002; Bradley *et al.*, 2012). Optical imaging systems have the potential to further influence the behavior of plankton through the illumination needed for imaging. The introduction of light has been shown to lure (Singarajah 1975) and mitigate the escape behavior of zooplankton (Wiebe *et al.*, 2004; Wiebe *et al.*, 2013). Therefore, *in situ*

instruments should be engineered to minimize the effects of light and hydrodynamic disturbances on the organisms they are observing.

Zooglider, a modified *Spray* glider (Sherman *et al.*, 2001), is novel in that it uses a low-power and completely autonomous acoustic (Zonar) and optical imaging system (Zoocam) (Ohman *et al.*, 2019). The Zoocam captures images at 2 Hz, while the Zonar concurrently records acoustic backscatter at two frequencies (200 kHz and 1000 kHz). *Zooglider* resolves both biological (e.g. zooplankton, phytoplankton, marine snow, and chlorophyll-*a* fluorescence) and physical properties (temperature, salinity, and pressure) at a vertical resolution of ∼5 cm. It is important to note that the Zoocam utilizes a specially designed sampling tunnel that effectively traps organisms and particles, well ahead of the *Zooglider*. The geometry of the sampling tunnel, as well as the placement of the Zoocam on the glider hull, was arrived at after a series of numerical simulations using Solidworks Flow Simulation (Ohman *et al.*, 2019). The design intent was to minimize the effects of shear in simulated flows up to 25 cm s^{-1} and to shield the organisms from the Zoocam illumination until they are well within the tunnel. Moreover, the wavelength of light was selected to be in the red part of the spectrum where crustacean eyes are relatively insensitive (see Ohman *et al.*, 2019 for details). The efficacy of these design features in natural ocean conditions is evaluated in the present manuscript.

The goal of the present study is to compare *Zooglider* measurements of the plankton assemblage with conventional net-based sampling (MOCNESS) and shipboard acoustic (Simrad EK80) measurements. We sought to determine the comparability between methods and to identify the limitations of each system. We compare the taxon-specific abundances, concentrations and size distributions of organisms detected by the Zoocam in comparison with MOCNESS-collected zooplankton and, separately, the volume backscatter reported by the two acoustic systems.

METHOD

For a full description of *Zooglider* engineering details, please see Ohman *et al.*, 2019.

Zooglider was deployed near La Jolla Canyon offshore of San Diego, California from 9–16 March 2017. The R/V *Sally Ride* was near *Zooglider's* last successive reported positions from 11–13 March 2017 (Fig. 1). Mean and maximum distances between the active Zonar dives and EK80 track, active Zoocam dives and MOCNESS tows and conductivity–temperature–depth (CTD) Casts and *Zooglider* dives were ∼2.42 km, 1.83 km and 1.40 km and 3.3 km, 2.2 km and 1.45 km, respectively. Distances were calculated using the ship and *Zooglider* GPS at each surfacing. As a safety precaution it was necessary to avoid lowering equipment in close proximity to *Zooglider*.

The *Sally Ride* was equipped with a five-frequency (18, 38, 70, 120 and 200) Simrad EK80, which was active for the duration of the cruise. The Zonar was active for 14 dives that corresponded in time and space with the *Sally Ride's* EK80. The Zonar was in listening mode for one dive off station for the purpose of background noise estimation. The Zoocam was active for nine dives from 11–13 March 2017. *Zooglider* dives were made at 3-h intervals continuously while on station near La Jolla Canyon. Each dive was to a depth of 400 m, and data were collected solely during the ascent portion of the dive.

Two-day and two-night 1-m^2 Multiple Opening/Closing Net and Environmental Sensing System (MOCNESS) tows were conducted from 400 m to the surface. The MOCNESS had 10 202-μm nets and was equipped with a front mounted CTD, Chl-*a* fluorometer, transmissometer and a calibrated flow meter. The 202-μm mesh size was chosen as *Zooglider* was initially designed to target mesozooplankton ranging in size from 0.45–20 mm. CTD casts were conducted ∼0.5 km away from the *Zooglider*'s last surfacing to collect water for extracted Chl-*a* vertical distributions. Each MOCNESS tow began ∼2 km south of the *Zooglider*'s last reported location and was towed with the same heading as the *Zooglider*. The goal of each tow was to maintain a speed over ground of 0.75–1.0 m s^{-1} and a MOCNESS net angle of 45°. Net 0 of the MOCNESS was open for the descent and beginning ascent of the tow and was closed at 400 m. The MOCNESS was towed obliquely from 400 m to the surface, and nets were tripped sequentially at predetermined depths that were consistent for all four tows. For all tows, nets 1–9 sampled consistent depth intervals (∼400-350-250-200-150-100-60-40-20-0 m) from 400 m to the surface. The smaller depth intervals near the surface (nets 7–9) were used to better define the structure of the upper layers of the water column. MOCNESS samples from nets 1–9 were immediately rinsed then preserved in a 1.8% solution of formaldehyde buffered with sodium tetraborate for post-processing on land.

Data analysis

MOCNESS samples were processed using the ZooScan flatbed scanner and ZooProcess software (Gorsky *et al.*, 2010). Each net sample was passed through three sieves (5 mm, 1 mm and 0.202 mm) for size fractionation. Each size fraction was then subsampled, using a Folsom splitter or Stempel pipette, into smaller aliquots based on the amount of material present within the sample.

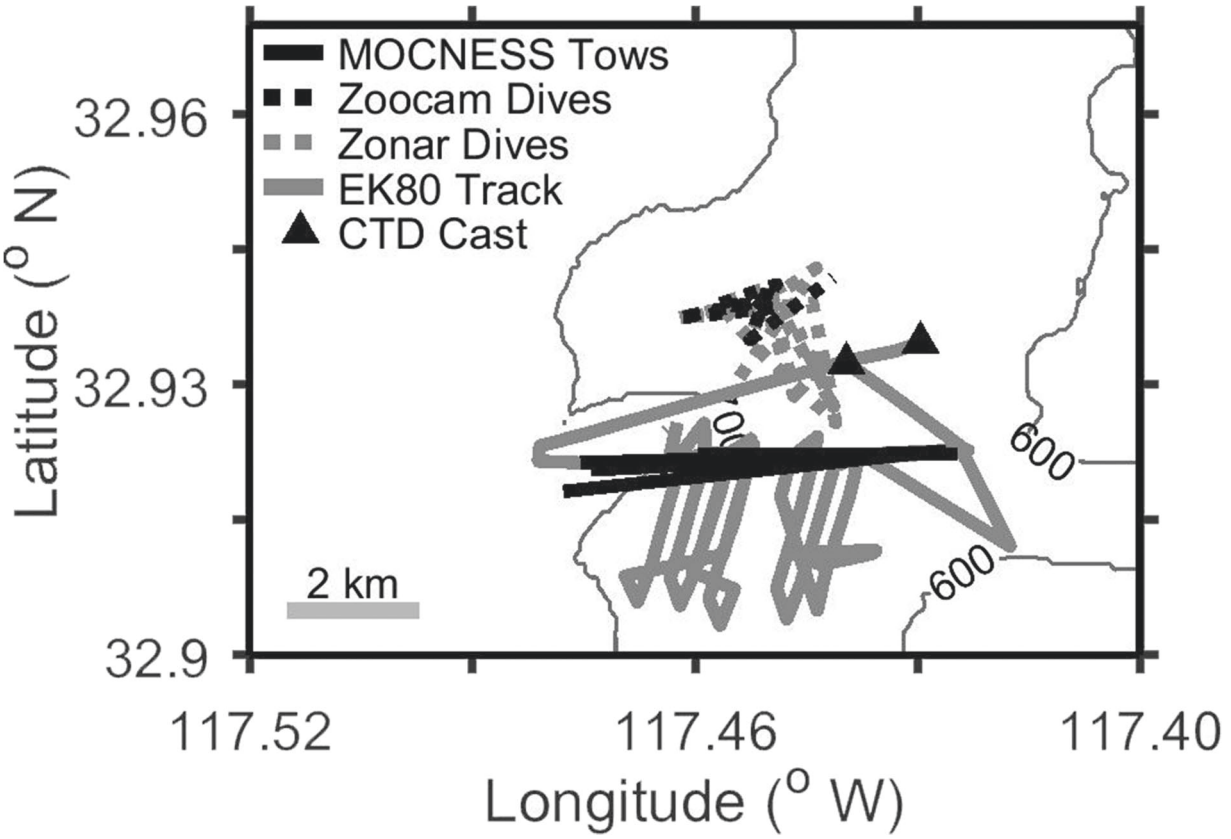

Fig. 1. The locations of the CTD casts (triangles), EK80 survey (gray solid line), Zonar dives (gray dotted line), Zoocam dives (black dotted line) and MOCNESS tows (black solid line).

The aliquots were then scanned, imaged, segmented and cropped into individual regions of interest (ROI) using ZooProcess. A total of 68 geometric features (e.g. area, min/mean/max intensity, etc.) were calculated for each ROI. The pixel resolution of the ZooScan is 10.6 μm pixel^{-1}, and the minimum threshold for a ROI to be counted and cropped is 0.45 mm equivalent circular diameter (ECD). The measured ROIs were pre-sorted into 26 categories by a Random Forest algorithm; then classifications of 100% of the images were manually confirmed. Each confirmed ROI was scaled by appropriate aliquot factors and the volume of water filtered *in situ* to obtain organismal densities as number m^{-3}.

The *Zooglider* CTD and fluorescence measurements were collected at different frequencies than the Zoocam images: 8 s and 0.5 s, respectively; so the CTD and fluorescence data were linearly interpolated using the Zoocam image timestamps. The Zoocam images were 1.2 MB (960 × 1280 pixels), with an image resolution of 40 μm pixel^{-1} and a sample volume of 250 mL image^{-1}. The raw Zoocam images were flat fielded to allow for consistent illumination across the frame (Ohman *et al.* 2019). The flat-fielded images were passed through a dual-pass image detection and segmentation algorithm based on Canny (1986) in order to identify ROIs within each image. Each ROI had 70 geometric features calculated and embedded in XMP format within the image, together with the interpolated physical data from *Zooglider* (Ellen, 2018). The threshold for a ROI to be cropped and saved was 0.45 mm ECD. The 0.45 mm threshold was found to be the smallest identifiable target size after several thousand frames of testing. The cropped ROIs were manually sorted into 57 categories.

To ascertain whether *Zooglider* and ship-based instruments were sampling the same water parcel, we compared ship-based and *Zooglider* mounted CTD profiles, as potential density (σ_θ), and chlorophyll-*a in vivo* fluorescence among the *Zooglider*, MOCNESS and CTD fluorometers, as well as the extracted chlorophyll-*a* from the CTD-rosette Niskin bottle samples. Water samples were filtered onto GFF filters, extracted in 90% acetone and analyzed with acidification on a Turner 10 AU fluorometer.

Eight taxa were compared between the MOCNESS samples and the *Zooglider in situ* images: Appendicularia, chaetognaths, *Oithona* (copepod), other Copepoda, euphausiids, gelatinous predators (Cnidaria and

Ctenophora), mineralized protists (Acantharia, Collodaria, Foraminifera, and Phaeodarea) and nauplii. These taxa were chosen because they had the greatest numbers of organisms within both the MOCNESS and *Zooglider* data sets.

The MOCNESS tows and *Zooglider* dives were divided into day and night samples to minimize expected diel differences in organismal concentrations. The day samples included two MOCNESS tows and five *Zooglider* dives, while the night samples included two MOCNESS tows and four *Zooglider* dives. Total abundances (No. m^{-2}) for the eight classes of organisms were vertically integrated from 400 m to the surface for both the *Zooglider* and MOCNESS data. These abundances were compared using a two-sample paired *t*-test (ttest2, MATLAB). No difference was observed when the total abundance data were dichotomized by time of day for both the MOCNESS and *Zooglider*, thus all day and night sampling was pooled for each sampling system and reanalyzed for differences in the total abundances.

Vertical distributions of the concentration of organisms (No. m^{-3}) were generated for the day and night sampling of all eight taxa, for both sampling systems. The *Zooglider* vertical distributions were binned at two different levels: the same depth intervals as sampled by the MOCNESS nets and 25 cm. The first binning was done for a side-by-side comparison between the two systems, while the 25 cm bin shows the finer vertical structure resolvable by the *Zooglider*. While *Zooglider* is capable of resolving 5 cm bins, the vertical structure of the less abundant taxa was hard to discern when viewed at full resolution, but more apparent at the 25 cm bin size. To emphasize the fine vertical structure of each taxon in the upper part of the water column, the graphs at the 0.25 cm bin size were truncated to 0–200 dBar. For the MOCNESS net depth intervals, the vertical distributions were compared using a two-sample paired *t*-test (ttest2, MATLAB).

In addition to the computer-generated geometric measurements, the width of each ROI was manually measured in ImageJ in order to make direct comparisons between organism sizes from Zoocam and ZooScan. Care was taken to not measure the moveable parts of each organism such as grasping spines, setae, tentacles and antennae. It was necessary to measure these widths manually, as the ROIs had several characteristics that hindered consistent computer-generated width measurements (e.g. pose, existence of appendicularian houses and relatively transparent features of the organism). The measured widths (w) were used to generate taxon-specific normalized probability distributions for both the MOCNESS and *Zooglider* data sets. Each probability distribution used a bin width of 40 μm (the largest pixel resolution between the *ZooScan* and Zoocam images). The normalized frequency distributions were then compared using a Kolmogorov–Smirnov test (kstest2, MATLAB). The 40 μm bin width resulted in probabilities well below 0.01 at the upper size range of each taxa size distribution. When such small probabilities were found, the smallest probability values were summed into one size class as to avoid artificially increasing the number of size classes being compared.

The width distribution data were subdivided into three size categories: small ($w \leq 0.28$ mm, the diagonal of the net mesh), medium ($0.28 < w \leq 1$ mm) and large organisms ($w > 1$ mm). These size categories were combined with the vertical distribution data to view taxon-specific size differences by depth. These MOCNESS and *Zooglider* size-dependent concentrations by depth were compared using a two-sample paired *t*-test (ttest2, MATLAB).

Active acoustic analysis focused on 200 kHz as this was the only common frequency between the EK80 and Zonar. Both instruments were calibrated using a standard tungsten carbide reference sphere (Foote *et al.*, 1987). The EK80 transmitted at a rate of 23 kHz with a 1.024-ms pulse length. EK80 acoustic backscatter was analyzed in Myriax Echoview 8 software. Background noise was removed following De Robertis and Higginbottom (2007), with a signal-to-noise threshold of 10 dB, which limited the depth of analysis to 200 m for comparison between instruments. Zonar data were processed following Ohman *et al.* (2019). The Zonar used a 5 kHz sampling rate with a 6-ms pulse length. Backscatter data were analyzed over a range of 3–8.1 m from the Zonar transducer face. For both instruments, average profiles of mean volume backscattering strength (S_v, dB re 1 m^{-1}; details in Ohman *et al.*, 2019) were calculated for the time period of the upcast of each dive in 10-m vertical bins and compared via regression analysis (r^2 from polyfit and polyval, *P*-value from fitlm and analysis of variance, MATLAB) for daylight and night dives separately.

A potential source of disagreement between the Zonar and EK80 is the difference in the volume each instrument insonifies (Guihen *et al.*, 2014; Moline *et al.*, 2015). For comparison, we calculated the volume insonified between 7–8 m from the Zonar transducer (the widest insonified radius used from that instrument) and in 1-m deep bins from 7–200 m from the EK80 transducer using equation 1.

$$V = \left(\pi {r_2}^2 \frac{h_2}{3}\right) - \left(\pi {r_1}^2 \frac{h_1}{3}\right), \quad (1)$$

where V is the insonified volume in m^3, *r* is the insonified radius in m, *h* is the distance from the transducer in m, the subscript 1 denotes the values for the shallower bound of the bin and the subscript 2 denotes the deeper bound

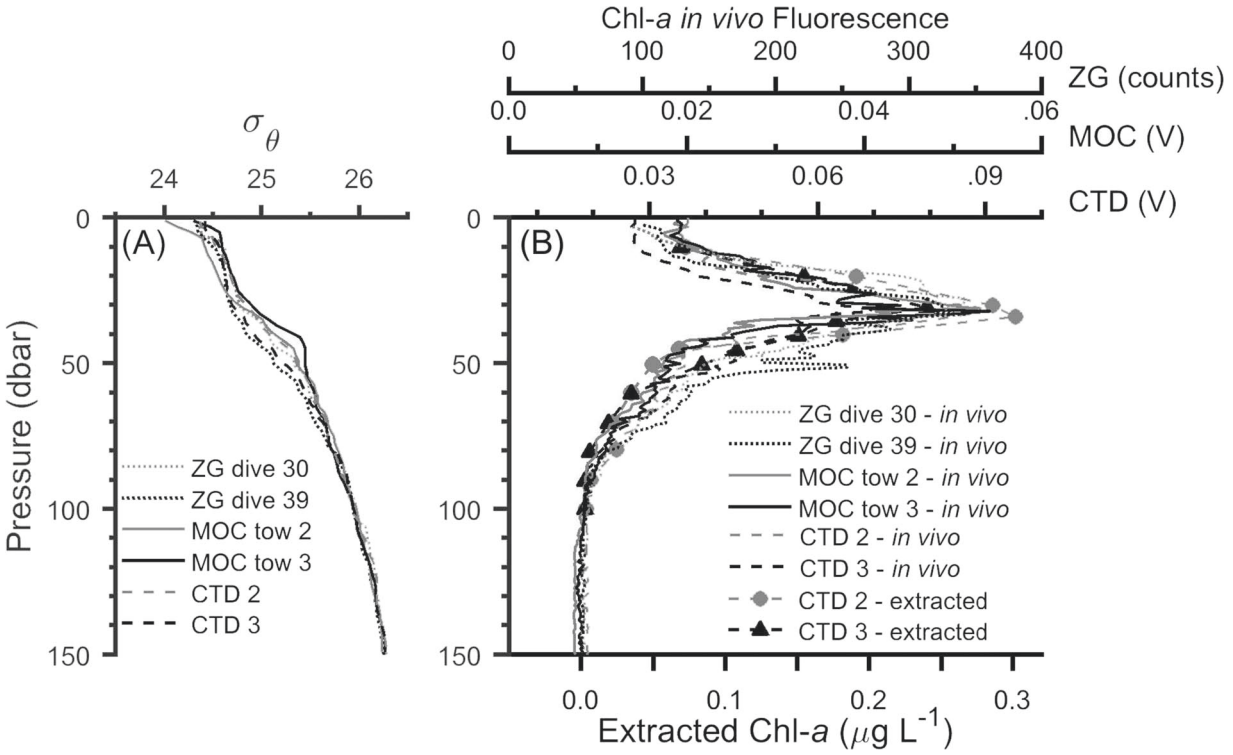

Fig. 2. *Zooglider*, MOCNESS and CTD-rosette measured (**A**) σ_θ and (**B**) Chl-*a in vivo* fluorescence (as digital counts, volts, and volts, respectively), together with extracted Chl-*a* (μg L^{-1}), plotted with respect to depth. The line color distinguishes the *Zooglider* dives, MOCNESS tows and CTD casts that were closest in time to one another.

of the bin. We calculated r using equation 2, where Ψ is the equivalent beam angle of the transducer in radians (0.17 rad for the Zonar and 0.12 rad for the EK80).

$$r = \Psi * h. \quad (2)$$

For analysis of the difference in insonified volumes between the two systems, we considered the ratio of EK80 sampling volume to the Zonar sampling volume as a function of depth.

RESULTS

The potential density profiles (Fig. 2a) from the CTD casts, MOCNESS tows and *Zooglider* dives correspond well, showing a relatively mixed layer from 10 m to 30 m. The extracted chlorophyll-*a* values from the CTD casts agree with the *in vivo* fluorescence measured by the CTD, MOCNESS and *Zooglider* fluorometers (Fig. 2b), with all sampling methods showing a sharply defined subsurface chlorophyll maximum between 30 m and 40 m, thus suggesting that we sampled similar water parcels with each instrument.

The vertically integrated abundances for all eight taxa are shown in Fig. 3. Significantly higher vertically integrated abundances were found for *Zooglider* relative to MOCNESS samples for other copepods ($P < 0.001$), *Oithona* ($P < 0.001$), appendicularians ($P < 0.01$), mineralized protists ($P < 0.01$) and gelatinous predators ($P < 0.05$). No difference was found for chaetognaths, euphausiids and nauplii ($P > 0.20$).

The vertical distributions for all taxa, when binned at MOCNESS net depth intervals (Fig. 4), show relatively consistent patterns of distribution by depth; however, the concentrations measured by *Zooglider* were typically much greater than the MOCNESS concentrations. Significant differences were observed between the MOCNESS and *Zooglider* concentration profiles for both the day and night profiles of other copepods ($P < 0.05$), *Oithona* ($P < 0.01$), appendicularians ($P < 0.05$), mineralized protists ($P < 0.001$) and gelatinous predators ($P < 0.05$ day, $P < 0.01$ night). No differences were detected for chaetognaths, euphausiids and nauplii ($P > 0.05$).

When the dives are examined individually at 0.05-dBar (5 cm) vertical intervals, markedly higher maximum concentrations were observed for all taxa, e.g. 53 000 other copepods m^{-3} and 29 000 appendicularians m^{-3} (not shown). However, as stated in the methods, at that resolution the relative scarcity of the other taxa makes it difficult for their vertical structure to be resolved from so few dives

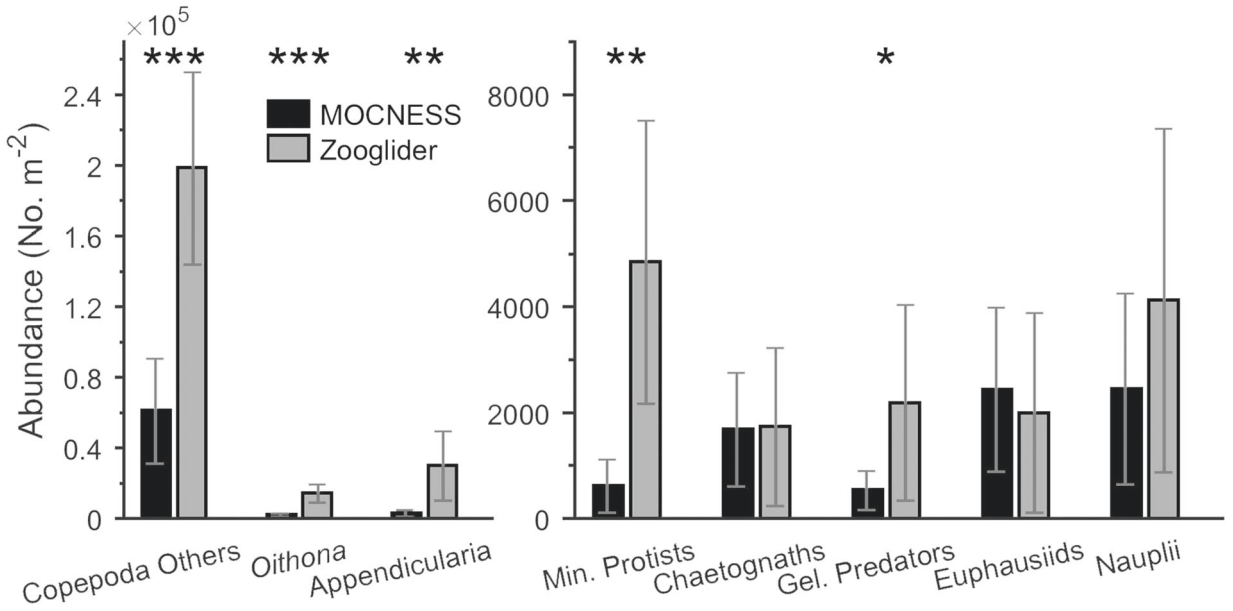

Fig. 3. Total abundances (No. m^{-2}, $\bar{x} \pm$ standard deviation) for all eight taxa as sampled by *Zooglider* (gray) and MOCNESS (black). Note the different y-label scales between the left and right columns. (* = $P < 0.05$; ** = $P < 0.01$; *** = $P < 0.001$).

because of abundant zero counts. When the vertical distributions for the *Zooglider* are instead binned at 0.25 dBar, the vertical microstructure becomes more clearly apparent, and the maximum concentrations remain greatly elevated relative to the MOCNESS measurements for all taxa (Supplementary Fig. 1). Chaetognaths appear to be relatively evenly distributed with respect to depth, while the other taxa typically show elevated concentrations between 0–75 dBar.

Normalized size distributions for the body widths of organisms for all eight taxa are shown in Fig. 5. Significant differences were found between the MOCNESS and *Zooglider* size distributions for mineralized protists ($P < 0.01$), gelatinous predators ($P < 0.01$), euphausiids ($P < 0.05$) and nauplii ($P < 0.05$). Other copepods, *Oithona*, appendicularians and chaetognaths showed no difference ($P > 0.05$) in size distributions. The vertical dotted line in Fig. 5 represents 0.28 mm, the diagonal measurement of the MOCNESS net mesh size.

Supplementary Fig. 2 shows the vertical distributions from Fig. 4 subdivided into three size groups based on organismal body width: small (0–0.28 mm), medium (0.28–1.0 mm) and large (>1.0 mm) with respective *P*-values, P_S, P_M and P_L. For the small size class, significant differences in concentrations between the MOCNESS and *Zooglider* ($P < 0.05$) were shown for other copepods (day only), *Oithona* and mineralized protists. The medium size class was significantly different for *Oithona* ($P < 0.001$ day; $P < 0.05$ night), appendicularians ($P < 0.05$) and mineralized protists ($P < 0.01$). The large size classes showed significant differences ($P < 0.05$ day; $P < 0.01$ night) for gelatinous predators and euphausiids. The remaining size classes showed no differences in concentrations between the MOCNESS and *Zooglider*.

Average day and night vertical profiles for acoustic volume backscatter at 200 kHz from the EK80 and Zonar are shown in Fig. 6A and B, respectively. The two instruments generally agree in pattern and magnitude of acoustic backscatter, although agreement was markedly better at night ($r^2 = 0.58$, $P < 0.001$) when depth variability of scatters was lower than during the day ($r^2 = 0.21$, $P < 0.05$). When comparing the volume backscatter of the two instruments within the upper 200 m, the volumes insonified are substantially different, with the surface-mounted EK80 insonifying ~350 times the volume of the Zonar at a depth of 200 m (Fig. 6C).

DISCUSSION

As to be expected, there were subtle variations in both the physical and biological properties as sampled by the multiple *Zooglider* dives, MOCNESS tows and CTD profiles. However, to properly address the potential influence of these variations in water column properties, as well as zooplankton patchiness on a broad spectrum of spatial scales (e.g. Haury *et al.*, 1978), on the organisms sampled many additional profiles and transects would be necessary and are beyond the scope of the present study. The general correspondence in potential density suggests that

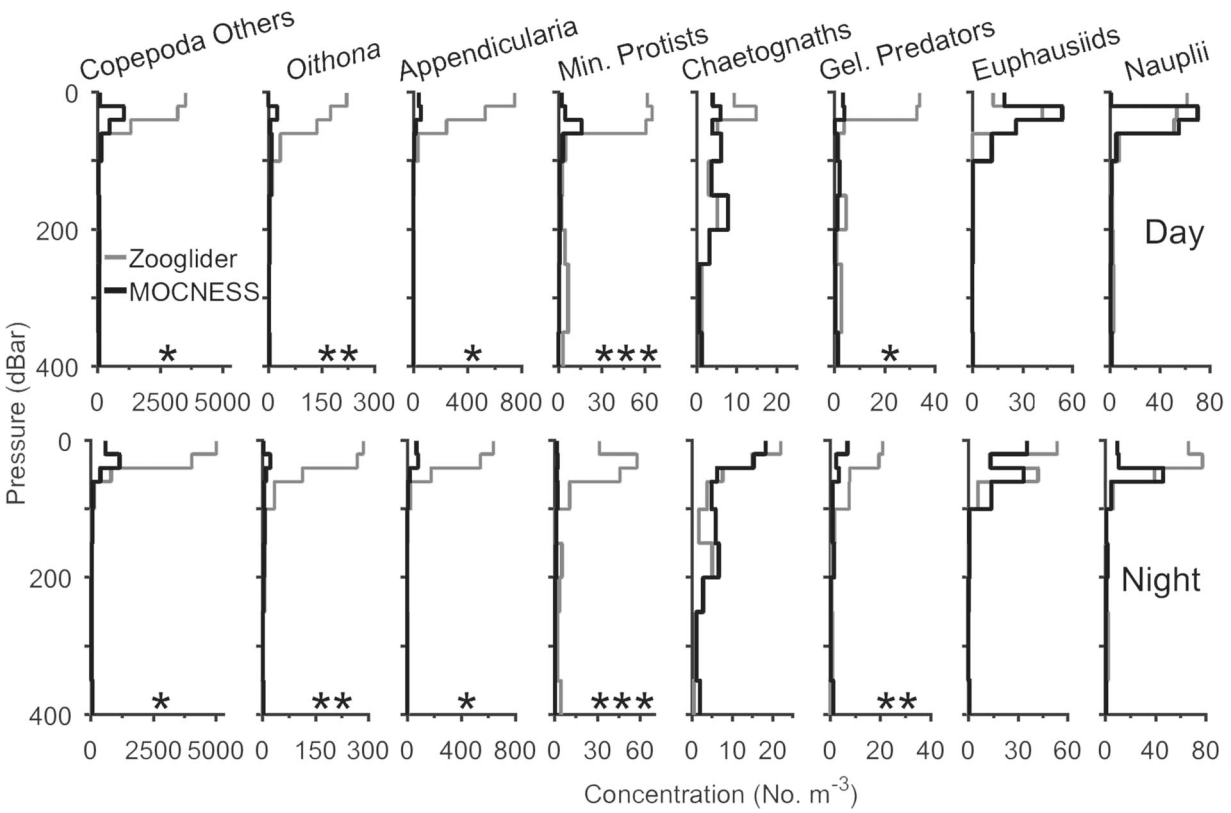

Fig. 4. Vertical distributions of organismal concentrations for MOCNESS (black) and *Zooglider* (gray) samples. Data were binned at the MOCNESS depth intervals by day (upper row) and night (lower row). (* = $P < 0.05$; ** = $P < 0.01$; *** = $P < 0.001$).

water parcels sampled by the CTD, MOCNESS and *Zooglider* had similar physical properties. The agreement in chlorophyll-*a* profiles suggests that the water parcels sampled by both the *Zooglider* and the instruments aboard the R/V *Sally Ride* bore similar biological characteristics. These similarities are supported by the proximity of the *Zooglider* to the R/V *Sally Ride* and minimal time difference between dives and MOCNESS tows (±3 h).

Zooglider and MOCNESS agreed on the abundances of taxa relative to one another within the water column (i.e. other copepods, appendicularians, and *Oithona* as the most abundant). However, there were stark differences between the MOCNESS and *Zooglider* measurements with regards to total abundance, concentrations and size distributions for many of the taxa. *Zooglider* showed significantly higher vertically integrated abundances and local concentrations for five of the eight taxa compared to the MOCNESS. There were significant differences between the two systems in the size distributions for four of the eight taxa. It should be recalled that *Zooglider* images organisms alive, *in situ*, while the MOCNESS/ZooScanned samples reflect both net capture and preservation artifacts, which could account for some of the size differences.

Previous studies have yielded similar results to *Zooglider*, concerning taxon-specific discrepancies in abundance, when comparing optical imaging systems to nets. The VPR showed discrepancies in numerical concentrations for medusae, appendicularians and copepods by factors of 360, 16.4 and 2.9, respectively (Benfield *et al.*, 1996). The Shadowed Image Particle Profiling and Evaluation Recorder revealed that a 162-μm mesh net significantly underestimated the abundance of appendicularians (300%), doliolids (379%), protists (522%) and ctenophores/cnidarians (1200%), but no significant differences in chaetognaths, copepods or euphausiids were detected (Remsen *et al.*, 2004). These differences in taxon abundance, or lack thereof, are primarily attributable to differences in net extrusion or robustness of different organisms and in particular whether they are fragile, soft-bodied or hard-bodied taxa. We believe that these results cannot be explained by light attraction of organisms because (i) red light was used to which the organisms are insensitive, (ii) the light source is recessed well inside the sampling tunnel and is difficult to discern and (iii) *Zooglider*'s ascent speed exceeds the sustained swimming capacity of small copepods (Wong 1988; Yen 1988) and most other

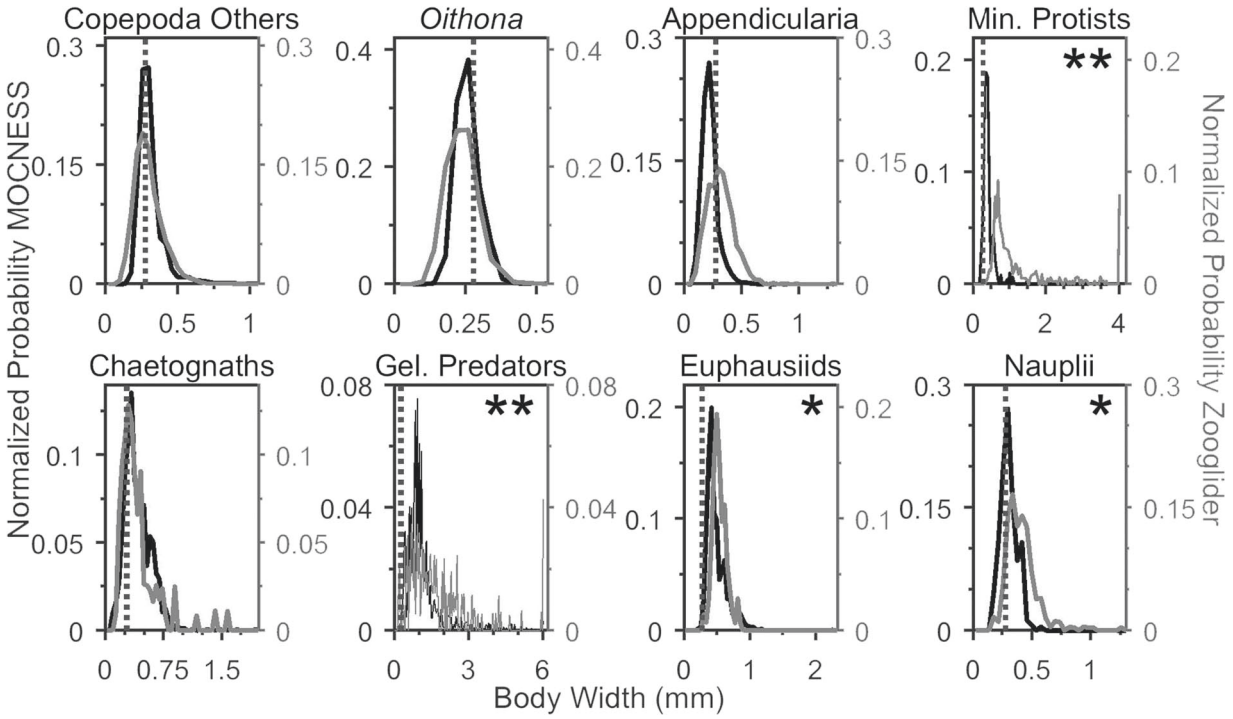

Fig. 5. Comparison of normalized size distributions of body widths for *Zooglider* (gray) and MOCNESS (black) samples, by taxon. The vertical dotted line represents 0.28 mm (the diagonal of the MOCNESS mesh size). (* = $P < 0.05$; ** = $P < 0.01$). For ease of viewing mineralized protists and gelatinous predators, probabilities were pooled for body widths exceeding 4 mm and 6 mm, respectively.

zooplankton (De Robertis *et al.*, 2003; Seuront *et al.*, 2004; Genin *et al.*, 2005).

The harder-bodied copepods are less likely to experience significant shrinkage due to preservation, thus any size discrepancies are most likely attributable to the sampling process. The majority of the *Oithona* that were captured by both systems were small, below 0.28 mm in body width, which is the open dimension of the diagonal of the net mesh (vertical dotted line; Fig. 5). It is likely that although the size distributions did not differ significantly, many *Oithona* were extruded through the MOCNESS 202-μm mesh with the added force of the water flowing through the net. Presumably, the *Oithona* that were captured by the net were more likely to be oriented orthogonal to the mesh opening. Similar reasoning applies to the other copepods category. As the discrepancy in concentration continues to persist into the medium size category of other copepods (0.28–1 mm), it is likely that some copepods exceeding 0.28 mm in body width were also extruded but to a lesser extent. This is not the first study to find such conclusions. Di Mauro *et al.* (2009) showed that a 220-μm mesh underestimated the copepod *Oithona nana* by 96.29%, harpacticoid copepods by 96.52%, and copepodites (stage I–III) of small calanoids by 99.7% when compared to a 67-μm mesh. Copepods with prosome lengths less than 550 μm were most efficiently sampled by a 64-μm mesh off the central coast of California (Hopcroft *et al.*, 2001).

The higher abundances and concentrations of appendicularians and gelatinous predators detected by *Zooglider* are also attributable to net extrusion; however, due to the softer bodies of these particular taxa, it is likely that the size range for extrusion may be higher than that of the harder-bodied copepods. Di Mauro *et al.* (2009) found that the soft-bodied appendicularian *Oikopleura dioica* was significantly underestimated for trunk lengths <500 μm with 220-μm mesh nets. Furthermore, appendicularians and gelatinous predators (here cnidarians and ctenophores) are more susceptible to degradation via net collection and formaldehyde-induced shrinkage and distortion (Nishikawa and Terazaki 1996; Beaulieu *et al.*, 1999), which in turn makes those degraded samples more difficult to identify and count for abundance estimates.

Soft-bodied zooplankton are not the only organisms that are distorted by net collection and preservation. The fragile pseudopodia and spines of mineralized protists are often destroyed or degraded by the processes of net collection, rinsing and fixation at sea. In the case of acantharians, their strontium sulfate spines are well known to dissolve in preservatives if sufficient strontium chloride is not added (Beers and Stewart 1970). Evidence of such

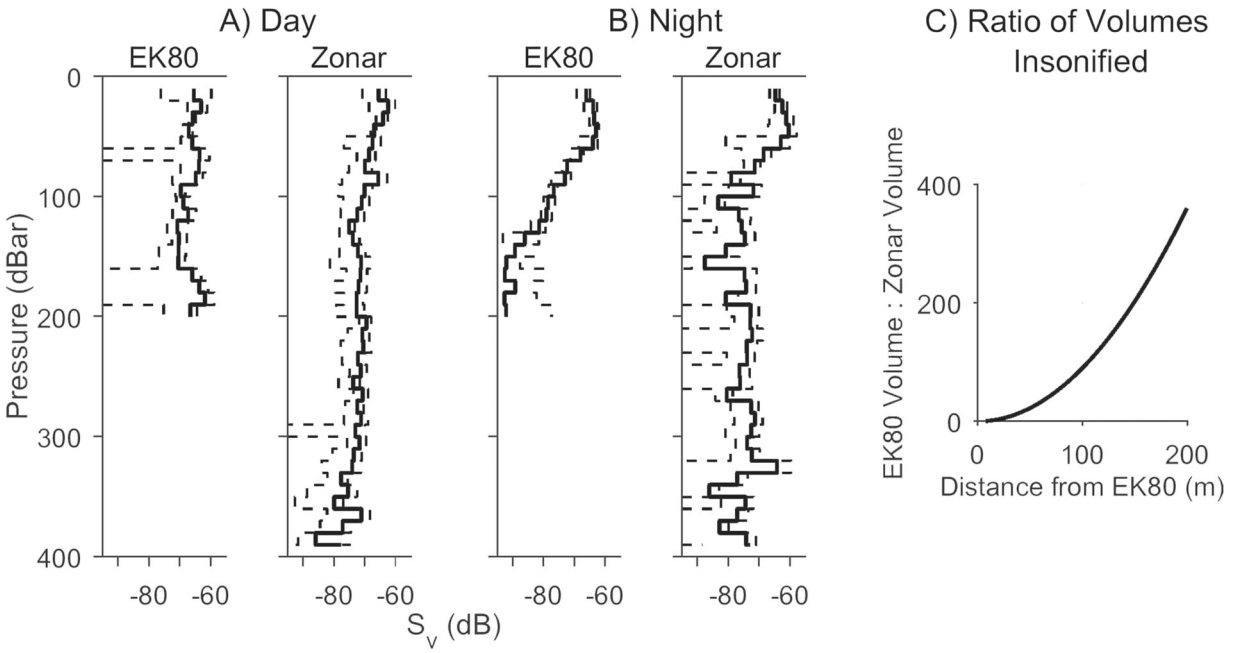

Fig. 6. Vertical distributions of 200 kHz volume backscatter (S_v) from the EK80 and Zonar, binned at 10 dBar, in (**A**) day and (**B**) night profiles. The vertical distributions of S_v from the two instruments were correlated both by day ($P < 0.05$) and by night ($P < 0.001$). Gray dotted lines enclose 95% confidence interval. Where the lower confidence bound goes out of the frame, the value was negative in linear space and has been set to an arbitrarily low number (−999) in log space. (**C**) Ratio of volume insonified by the ship-mounted EK80 to *Zooglider*-mounted Zonar, as a function of increasing *Zooglider* depth. The Zonar volume remains constant with depth, while the EK80 volume increases.

sample degradation was clearly observed in the MOCNESS samples, as no mineralized protists (also including phaeodarians, foraminifera and collodarians) retained their spines or pseudopodia. This degradation can render mineralized protists too small to be saved by our 0.45-mm ECD threshold and hinder their accurate classification, which would account for the size, concentration and abundance differences seen by *Zooglider*. In contrast to the degradation associated with net samples, *Zooglider* images organisms in their natural posture within the water column, with delicate structures intact (Ohman *et al.*, 2019; Gaskell *et al.*, 2019). Accordingly, mineralized protists along with soft-bodied appendicularians and gelatinous predators are generally larger than their shrunken and broken preserved counterparts, which accounts for differences in size between the MOCNESS and *Zooglider* samples.

The abundance of nauplii did not differ between the two sampling approaches, although smaller nauplii made up a larger proportion of the MOCNESS samples compared to *Zooglider* samples. We believe this size discrepancy is due to the difference in pixel resolution between the two systems. The smaller appendages of many nauplii were more readily identifiable within the MOCNESS samples at the ZooScan resolution of 10.6 μm pixel^{-1}, while many possible nauplii were labeled 'unsure' due to the Zoocam resolution of 40 μm pixel^{-1} and therefore not included in the nauplii data.

Chaetognaths were sampled with similar vertically integrated abundances, depth-specific concentrations and size distributions by the two methods. We presume that chaetognaths are less likely than fragile cnidarians, ctenophores and appendicularians to be damaged by net collection or to be extruded through the net mesh.

The MOCNESS and *Zooglider* captured similar abundances of euphausiids, with slightly larger body widths recorded by *Zooglider*. However, the very largest specimens we found were detected in MOCNESS net samples, albeit at very low abundances (<0.0001 animals m^{-3}). This size difference may be attributed to a relatively low abundance of large euphausiids within the water column, coupled with the discrepancies in sample volume between *Zooglider* and MOCNESS, or perhaps to avoidance behavior (*cf.*, Brinton, 1967). However, the euphausiids in Zoocam images are in natural postures and do not exhibit abdominal flexure typically associated with avoidance. Furthermore, the Zoocam utilizes a sampling tunnel that was designed specifically to minimize hydrodynamic disturbances that may trigger escape responses (Ohman *et al.*, 2019).

Zooglider was able to discern much greater concentrations and abundances of several taxa. When viewed

at small scales (<<1 m) maximum concentrations for other copepods and appendicularians reached 53 000 and 29 000 animals m^{-3}, respectively. The persistence and extent of these high concentrations will ultimately determine their effect on the planktonic community, a topic we will address in future publications.

The dual frequency Zonar records acoustic backscatter from smaller (1000 kHz) and larger zooplankton (200 kHz) and other organisms. However, the only acoustic frequency held in common between the Zonar and EK80 was 200 kHz; hence comparisons could only be made for the larger component of the acoustic backscatter. At 200 kHz, the vessel-mounted EK80 and *Zooglider*-mounted Zonar generally agree in magnitude and overall distribution of backscatter when averaged over all day and all night dives. Agreement was better at night when scatterers migrated to the surface and their distributions were less variable. The differences may be attributable to the difference in volume insonified between instruments. The detection probability for rare but strong scatterers would be higher for larger sampling volumes. An acoustic beam insonifies an approximately conical volume of water that widens with increasing distance from the instrument. The vessel-mounted EK80 only samples from the surface, and therefore the sampling volume increases proportionally with depth, while the Zonar sampling volume remains constant. Thus, the larger rare, strong scatterers will be better represented in the EK80 backscatter data. However, the EK80 200 kHz has an effective depth sampling limit of 200 m due to a decline in the signal-to-noise ratio (SNR) in deeper depths. Conversely, the profiling glider-mounted Zonar permits the effective sampling of much deeper water than vessel-mounted echosounders (Guihen *et al.*, 2014; Moline *et al.*, 2015; Powell and Ohman 2015). The acoustic systems were not compared with the imaging and net collections in this study as that would require information regarding taxon-specific acoustic scattering models, frequency-dependent acoustic target strength and orientation of the organisms insonified (Briseño-Avena *et al.*, 2015).

CONCLUSION

Zooglider captures greater numbers of smaller-sized organisms (i.e. copepods and appendicularians) and larger-sized organisms (i.e. mineralized protists, medusa, siphonophores and ctenophores) compared to the MOCNESS. Comparable abundances and similar size distributions are found for other taxa (chaetognaths, euphausiids and nauplii). A combination of net extrusion, net-induced damage and preservation effects all contribute to these abundance and size discrepancies. *Zooglider* was able to resolve elevated concentrations of copepods and appendicularians, to 53 000 and 29 000 animals m^{-3}, respectively. The Zonar agrees with the EK80 in magnitude and overall distribution of acoustic backscatter at 200 kHz. The profiling nature of the *Zooglider* allows it to sample much deeper than vessel-mounted echosounders without losing sample resolution due to a decline in SNR. *Zooglider*'s acoustic and optical sensing systems, in combination with its autonomy and endurance, make it uniquely capable to sample zooplankton distributions with minimal disruption to the organisms.

SUPPLEMENTARY DATA

Supplementary data can be found at *Journal of Plankton Research* online.

ACKNOWLEDGEMENTS

The Instrument Development Group (R. Davis, J. Sherman, K. Grindley, B. Rieneman, E. Goodwin and D. Vana) is to be credited with the design and manufacture of *Zooglider*. We thank UC Ship Funds for research vessel time and the crew of the R/V *Sally Ride*. E. Tovar ZooScanned the MOCNESS samples, J. Ellen assisted with post-processing of the Zoocam images and J. Trickey assisted with EK80 processing.

FUNDING

Gordon and Betty Moore Foundation (3576 and 5479); CCE-LTER (NSF OCE-16-37632); DoD SMART fellowship; UC Ship Funds for the award of ship-time.

REFERENCES

Beaulieu, S. E., Mullin, M. M., Tang, V. T., Pyne, S. M., King, A. L. and Twining, B. S. (1999) Using an optical plankton counter to determine the size distributions of preserved zooplankton samples. *J. Plankton Res.*, **21**, 1939–1956.

Beers, J. R. and Stewart, G. L. (1970) The preservation of acantharians in fixed plankton samples. *Limnol. Oceanogr.*, **15**, 825–827.

Benfield, M. C., Davis, C. S., Wiebe, P. H., Gallager, S. M., Lough, R. G. and Copley, N. J. (1996) Video Plankton Recorder estimates of copepod, pteropod and larvacean distributions from a stratified region of Georges Bank with comparative measurements from a MOCNESS sampler. *Deep Sea Res., Part II*, **43**, 1925–1945.

Benoit-Bird, K. J. (2009) Dynamic 3-dimensional structure of thin zooplankton layers is impacted by foraging fish. *Mar. Ecol. Prog. Ser.*, **396**, 61–76.

Bradley, C. J., Strickler, J. R., Buskey, E. J. and Lenz, P. H. (2012) Swimming and escape behavior in two species of calanoid copepods from nauplius to adult. *J. Plankton Res.*, **35**, 49–65.

Brentnall, S. J., Richards, K. J., Brindley, J. and Murphy, E. (2003) Plankton patchiness and its effect on larger-scale productivity. *J. Plankton Res.*, **25**, 121–140.

Brinton, E. (1967) Vertical migration and avoidance capability of euphausiids in the California Current. *Limnol. Oceanogr.*, **12**, 451–483.

Briseño-Avena, C., Roberts, P. L. D., Franks, P. J. S. and Jaffe, J. S. (2015) ZOOPS-O2: a broadband echosounder with coordinated stereo optical imaging for observing plankton in situ. *Methods in Oceanography*, **12**, 36–54.

Buskey, E. J., Lenz, P. H. and Hartline, D. K. (2002) Escape behavior of planktonic copepods in response to hydrodynamic disturbances: high speed video analysis. *Mar. Ecol. Prog. Ser.*, **235**, 135–146.

Canny, J. (1986) A computational approach to edge detection. *IEEE Trans. Pattern Anal. Mach. Intell.*, **PAMI-8**, 679–698.

Checkley, D. M. J., Ortner, P. B., Settle, L. R. and Cummings, S. R. (1997) A continuous, underway fish egg sampler. *Fish. Oceanogr.*, **6**, 58–73.

Cowen, R. K. and Guigand, C. M. (2008) In situ ichthyoplankton imaging system (ISIIS): system design and preliminary results. *Limnol. Oceanogr. Methods*, **6**, 126–132.

Davis, C. S., Thwaites, F. T., Gallager, S. M. and Hu, Q. (2005) A three-axis fast-tow digital Video Plankton Recorder for rapid surveys of plankton taxa and hydrography. *Limnol. Oceanogr. Methods*, **3**, 59–74.

De Robertis, A. and Higginbottom, I. (2007) A post-processing technique to estimate the signal-to-noise ratio and remove echosounder background noise. *ICES J. Mar. Sci.*, **64**, 1282–1291.

De Robertis, A., Schell, C. and Jaffe, J. S. (2003) Acoustic observations of the swimming behavior of the euphausiid *Euphausia pacifica* Hansen. *ICES J. Mar. Sci.*, **60**, 885–898.

Dekshenieks, M. M., Donaghay, P. L., Sullivan, J. M., Rines, J. E., Osborn, T. R. and Twardowski, M. S. (2001) Temporal and spatial occurrence of thin phytoplankton layers in relation to physical processes. *Mar. Ecol. Prog. Ser.*, **223**, 61–71.

Di Mauro, R., Capitanio, F. and Viñas, M. D. (2009) Capture efficiency for small dominant mesozooplankters (Copepoda, Appendicularia) off Buenos Aires Province (34°S–41°S), Argentine Sea, using two plankton mesh sizes. *Braz. J. Oceanogr.*, **57**, 205–214.

Ellen, J. (2018) Improving biological object classification in plankton images using convolutional neural networks, geometric features, and context metadata. *PhD Thesis*. University of California, San Diego.

Fields, D. M. and Yen, J. (1997) The escape behavior of marine copepods in response to a quantifiable fluid mechanical disturbance. *J. Plankton Res.*, **19**, 1289–1304.

Foote, K. G., Knudsen, H. P., Vestnes, G., MacLennan, D. N., and Simmonds, E. J. (1987) Calibration of acoustic instruments for fish density estimation: a practical guide. *ICES Coop. Res. Rep.*, **144**, 1–69.

Gaskell, D. E., Ohman, M. D. and Hull, P. M. (2019) Zooglider-based measurements of planktonic foraminifera in the California Current System. *J. Foram. Res.*, in press.

Genin, A., Jaffe, J.S., Reef, R., Richter, C. and Franks, P.J. (2005) Swimming against the flow: a mechanism of zooplankton aggregation. *Science*, **308**(5723), 860–862.

Gorsky, G., Ohman, M. D., Picheral, M., Gasparini, S., Stemmann, L., Romagnan, J.-B., Cawood, A., Pesant, S. *et al.* (2010) Digital zooplankton image analysis using the ZooScan integrated system. *J. Plankton Res.*, **32**, 285–303.

Griffiths, G., Fielding, S. and Roe, H. S. (2002) Biological–physical–acoustical interactions. *The Sea*, **12**, 441–474.

Grosjean P. and Denis K. (2007) ZooImage User's Manual. http://www.sciviews.org/zooimage/index.html, last accessed on 6 March 2019.

Guihen, D., Fielding, S., Murphy, E. J., Heywood, K. J. and Griffiths, G. (2014) An assessment of the use of ocean gliders to undertake acoustic measurements of zooplankton: the distribution and density of Antarctic krill (Euphausia superba) in the Weddell Sea. *Limnol Oceanogr. Methods*, **12**, 373–389.

Hamner, W., Madin, L., Alldredge, A., Gilmer, R. and Hamner, P. (1975) Underwater observations of gelatinous zooplankton: sampling problems, feeding biology, and behavior. *Limnol. Oceanogr.*, **20**, 907–917.

Haury, L., Mcgowan, J. and Wiebe, P. (1978) Patterns and processes in the time-space scales of plankton distributions. In *Spatial Pattern in Plankton Communities*, Springer, Boston, MA, USA, pp. 277–327.

Haury, L. R., Kenyon, D. E., and Brooks, J. R. (1980) Experimental evaluation of the avoidance reaction of Calanus finmarchicus. *J. Plankton Res.*, **2**, 187–202.

Herman, A., Beanlands, B. and Phillips, E. (2004) The next generation of optical plankton counter: the laser-OPC. *J. Plankton Res.*, **26**, 1135–1145.

Hopcroft, R., Roff, J. and Chavez, F. (2001) Size paradigms in copepod communities: a re-examination. *Hydrobiologia*, **453**, 133–141.

McGehee, D., O'driscoll, R. L. and Traykovski, L. M. (1998) Effects of orientation on acoustic scattering from Antarctic krill at 120 kHz. *Deep Sea Res., Part II*, **45**, 1273–1294.

Menden-Deuer, S. and Grünbaum, D. (2006) Individual foraging behaviors and population distributions of a planktonic predator aggregating to phytoplankton thin layers. *Limnol. Oceanogr.*, **51**, 109–116.

Moline, M. A., Benoit-Bird, K., O'Gorman, D. and Robbins, I. C. (2015) Integration of scientific echo sounders with an adaptable autonomous vehicle to extend our understanding of animals from the surface to the bathypelagic. *J. Atmos. Ocean. Technol.*, **32**, 2173–2186.

Möller, K. O., John, M. S., Temming, A., Floeter, J., Sell, A. F., Herrmann, J.-P. and Möllmann, C. (2012) Marine snow, zooplankton and thin layers: indications of a trophic link from small-scale sampling with the Video Plankton Recorder. *Mar. Ecol. Prog. Ser.*, **468**, 57–69.

Nichols, J. and Thompson, A. (1991) Mesh selection of copepodite and nauplius stages of four calanoid copepod species. *J. Plankton Res.*, **13**, 661–671.

Nishikawa, J. and Terazaki, M. (1996) Tissue shrinkage of two gelatinous zooplankton, *Thalia democratica* and *Dolioletta gegenbauri* (Tunicata: Thaliacea) in preservative. *Bull. Plankton Soc. Jpn*, **43**, 1–7.

Ohman, M. D., Davis, R., Sherman, J. T., Grindley, K. R., Whitmore, B. M., Nickels, C. F., and Ellen, J. S. (2019) Zooglider: an autonomous vehicle for optical and acoustic sensing of zooplankton. *Limnol. Oceanogr.: Methods*, **17**, 69–86. doi: 10.1002/lom3.10301.

Omori, M. and Hamner, W. (1982) Patchy distribution of zooplankton: behavior, population assessment and sampling problems. *Mar. Biol.*, **72**, 193–200.

Picheral, M., Guidi, L., Stemmann, L., Karl, D. M., Iddaoud, G. and Gorsky, G. (2010) The Underwater Vision Profiler 5: an advanced instrument for high spatial resolution studies of particle size spectra and zooplankton. *Limnol. Oceanogr. Methods*, **8**, 462–473.

Pinel-Alloul, B. and Ghadouani, A. (2007) Spatial heterogeneity of planktonic microorganisms in aquatic systems. In *The Spatial Distribution of Microbes in the Environment*, Dordrect: Springer, pp. 203–310.

Prairie, J. C., Ziervogel, K., Camassa, R., Mclaughlin, R. M., White, B. L., Dewald, C. and Arnosti, C. (2015) Delayed settling of marine snow: effects of density gradient and particle properties and implications for carbon cycling. *Mar. Chem.*, **175**, 28–38.

Pitois, S. G., Bouch, P., Creach, V. and Van Der Kooij, J. (2016) Comparison of zooplankton data collected by a continuous semi-automatic sampler (CALPS) and a traditional vertical ring net. *J. Plankton Res.*, **38**, 931–943.

Powell, J. R. and Ohman, M. D. (2015) Changes in zooplankton habitat, behavior, and acoustic scattering characteristics across glider-resolved fronts in the Southern California current system. *Prog. Oceanogr.*, **134**, 77–92.

Roberts, P. L., Jaffe, J. S., Orenstein, E. C., Laxton, B., Franks, P. J. S., Briseno, C., Carter, M. L. and Hilbern, M. (2014) *Pier Recognition: An In Situ Plankton Web Camera*, Ocean Optics XXII, Portland, ME, USA.

Remsen, A., Hopkins, T. L. and Samson, S. (2004) What you see is not what you catch: a comparison of concurrently collected net, Optical Plankton Counter, and Shadowed Image Particle Profiling Evaluation Recorder data from the Northeast Gulf of Mexico. *Deep Sea Res., Part I*, **51**, 129–151.

Rovinsky, A. B., Adiwidjaja, H., Yakhnin, V. Z. and Menzinger, M. (1997) Patchiness and enhancement of productivity in plankton ecosystems due to the differential advection of predator and prey. *Oikos*, **78**, 101–106.

Schulz, J., Barz, K., Mengedoht, D., Hanken, T., Lilienthal, H., Rieper, N., Hoops, J., Vogel, K. *et al.* (2009) Lightframe on-sight key species investigation (LOKI). OCEANS 2009-EUROPE, Bremen, Germany, IEEE, pp. 1–5.

Seuront, L., Yamazaki, H. and Souissi, S., 2004. Hydrodynamic disturbance and zooplankton swimming behavior. *Zool. Stud.,* **43**(2), 376–387.

Sheng, J., Malkiel, E. and Katz, J. (2003) Single beam two-views holographic particle image velocimetry. *Appl. Opt.*, **42**, 235–250.

Sherman, J., Davis, R. E., Owens, W. and Valdes, J. (2001) The autonomous underwater glider "spray". *IEEE J. Oceanic Eng.*, **26**, 437–446.

Singarajah, K. V. (1975) Escape reactions of zooplankton: effects of light and turbulence. *J. Mar. Biol. Assoc. U.K.*, **55**, 627–639.

Skjoldal, H. R., Wiebe, P. H., Postel, L., Knutsen, T., Kaartvedt, S. and Sameoto, D. D. (2013) Intercomparison of zooplankton (net) sampling systems: results from the ICES/GLOBEC Sea-going workshop. *Prog. Oceanogr.*, **108**, 1–42.

Trevorrow, M. V., Mackas, D. L. and Benfield, M. C. (2005) Comparison of multifrequency acoustic and in situ measurements of zooplankton abundances in Knight Inlet, British Columbia. *J. Acoust. Soc. Am.*, **117**, 3574–3588.

Weikert, H. and John, H.-C. (1981) Experiences with a modified Bé multiple opening-closing plankton net. *J. Plankton Res.*, **3**, 167–176.

Wiebe, P., Boyd, S., Davis, B. and Cox, J. (1982) Avoidance of towed nets by the euphausiid Nematoscelis megalops. *Fish Bull*, **80**, 75–91.

Wiebe, P., Morton, A., Bradley, A., Backus, R., Craddock, J., Barber, V., Cowles, T. and Flierl, G. D. (1985) New development in the MOCNESS, an apparatus for sampling zooplankton and micronekton. *Mar. Biol.*, **87**, 313–323.

Wiebe, P. H. and Benfield, M. C. (2003) From the Hensen net toward four-dimensional biological oceanography. *Prog. Oceanogr.*, **56**, 7–136.

Wiebe, P. H., Ashjian, C. J., Gallager, S. M., Davis, C. S., Lawson, G. L., and Copley, N. J. (2004) Using a high-powered strobe light to increase the catch of Antarctic krill. *Mar. Biol.*, **144**, 493–502.

Wiebe, P. H., Lawson, G. L., Lavery, A. C., Copley, N. J., Horgan, E. and Bradley, A. (2013) Improved agreement of net and acoustical methods for surveying euphausiids by mitigating avoidance using a net-based LED strobe light system. *ICES J. Mar. Sci.*, **70**, 650–664.

Wilson, S. and Steinberg, D. (2010) Autotrophic picoplankton in mesozooplankton guts: evidence of aggregate feeding in the mesopelagic zone and export of small phytoplankton. *Mar. Ecol. Prog. Ser.*, **412**, 11–27.

Wong, C. K. (1988) The swimming behavior of the copepod *Metridia pacfica*. *J. Plankton Res.*, **10**, 1285–1290.

Yen, J. (1988) Directionality and swimming speeds in predator-prey and male-female interactions of *Euchaeta rimana*, a subtropical marine copepod. *Bull. Mar. Sci.*, **43**, 395–403.